Near-Field Channel Interpolation for Pilot Overhead Reduction in XL-MIMO

Heedong Do
Korea University, Korea
Email: doheedong@korea.ac.kr

Namyoon Lee
POSTECH, Korea
Email: nylee@postech.ac.kr

Angel Lozano
Univ. Pompeu Fabra (UPF), Spain
Email: angel.lozano@upf.edu

***Abstract*—This paper considers the reconstruction of near-field line-of-sight multiantenna channels from the estimation of the shape of the radio wavefronts giving rise to such channels. This wavefront estimation can be conducted from only partial observations, which amounts to channel interpolation and/or extrapolation in near-field conditions. A tradeoff then arises and is characterized between the number of antennas and frequency bands on which pilot symbols are transmitted, the power of those pilots, and the accuracy of the ensuing channel reconstruction.**

I. Introduction

The default approach to channel estimation in multiantenna wireless communication entails a direct estimation of the channel entries for each transmit-receive antenna pair at each frequency band [1], [2]. This approach, however, overlooks the low-dimensional nature of many such channels, whose entries are functions of a few propagation parameters, often of a geometric nature. Leveraging this high degree of structure can greatly reduce the estimation error [3].

Two persistent trends in the evolution of wireless technologies reinforce the appeal of leveraging the channel's structure. These are the growing antenna counts, pushing towards extra-large multiple-input multiple-output (XL-MIMO) architectures, and the broadening bandwidths. Together, they increase the channel dimensionality dramatically, yet the number of underlying parameters remains essentially unchanged.

While the most straightforward way to capitalize on the channel's structure is to estimate those underlying parameters themselves, this is exponentially complex in the number of such parameters [4]. Several parametric channel estimators have been set forth, which indeed exhibit superior accuracy, but are circumscribed to settings in which the number of parameters is at most three. This, in turn, severely limits the applicability: either linear transmit and receive arrays, or else a planar array communicating with a single antenna.

Alternatively, the channel's structure can be exploited by estimating the shape of the radio wavefronts. The number of coefficients required to describe the wavefronts, while slightly higher than the number of underlying parameters, still does not grow with the numbers of antennas or the bandwidth [4]. And, the computational complexity of wavefront estimation scales at most quadratically in the number of coefficients in the wavefront description, whereby the applicability of this approach becomes universal, extending all the way to planar transmit and receive arrays and multiple frequency bands.

Crucially, the shape of the wavefronts can be estimated from only partial observations and, subsequently, the entire XL-MIMO channel can be straightforwardly reconstructed.

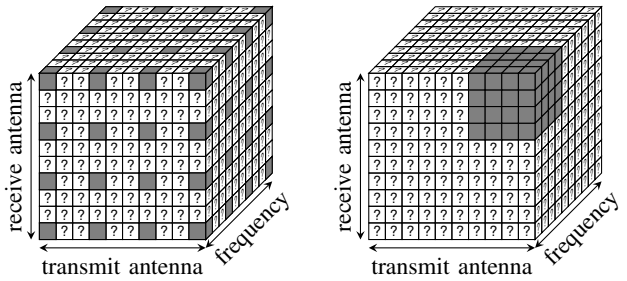

(a) Channel interpolation (b) Channel extrapolation

Fig. 1. Only the shaded entries are measured via pilot symbols; the unobserved entries can be inferred via interpolation or extrapolation.

This amounts to interpolating and/or extrapolating to unobserved points on an antenna-frequency grid, as illustrated in Fig. 1. The stage is then set for a major reduction in pilot overhead, and for a tradeoff between such overhead, the power of the pilot symbols, and the estimation accuracy.

While there is considerable literature on channel interpolation/extrapolation (see [5], [6] for frequency-domain techniques, or [7] for end-to-end learning methods), the bulk of it has been formulated for far-field conditions. However, the push towards XL-MIMO and to higher frequencies expand the near-field region [8]–[11], rendering obsolete any method developed exclusively for the far field. In contrast, a wavefront-based interpolator/extrapolator can operate in both far- and near-field conditions.

This paper focuses on links that are either line-of-sight (LOS) or embodied by a specular reflection [12]. From the series expansion of the distance between transmit and receive antennas, the wavefront is modelled as a multidimensional polynomial phase function [4]; this is a natural generalization of the popular parabolic wavefront model [13]. Uniformly sampling the channel on each dimension, as in Fig. 1(a), the result is again a polynomial phase function. This is the key observation that opens the door to near-field interpolation/extrapolation, and suggests the use of the polynomial phase estimator developed in [14], which attains the Cramer-Rao bound (CRB) at high signal-to-noise ratio (SNR).

A. Notation

The set of nonnegative integers is indicated by $\mathbb{N}_0$ whereas the first $N > 0$ nonnegative integers are compactly denoted by $[N] \equiv \{0, 1, \ldots, N-1\}$. Also used is the Iverson bracket

$$[\text{condition}] \equiv \begin{cases} 1 & \text{the condition is true} \\ 0 & \text{otherwise} \end{cases}. \tag{1}$$

$$a_{\boldsymbol{m}} = \begin{cases} d_{\mathrm{f}} c_{\boldsymbol{\ell}} & \boldsymbol{m} = (\boldsymbol{\ell}, 1) \text{ with } \boldsymbol{\ell} \in \mathcal{L} \\ 0 & \text{otherwise} \end{cases} \qquad p_{\boldsymbol{m}}(\boldsymbol{n}) = \begin{cases} \frac{(n_{\mathrm{r},x}, n_{\mathrm{r},y}, n_{\mathrm{t},x}, n_{\mathrm{t},y})^{\boldsymbol{\ell}}}{\boldsymbol{\ell}!} \left(\frac{1}{d_{\mathrm{f}}} + \left(n_{\mathrm{f}} - \frac{N_{\mathrm{f}}-1}{2} \right) \right) & \boldsymbol{m} = (\boldsymbol{\ell}, 1) \text{ with } \boldsymbol{\ell} \in \mathcal{L} \\ \frac{\boldsymbol{n}^{\boldsymbol{m}}}{\boldsymbol{m}!} & \text{otherwise} \end{cases} \tag{10}$$

There should be no confusion between these bracket notations, as their arguments are of a different nature. In addition, given $\boldsymbol{N} = (N_0, \dots, N_{\mathsf{D}-1}) \in \mathbb{Z}^{\mathsf{D}}$, we define $[\boldsymbol{N}] \equiv [N_0] \times \cdots \times [N_{\mathsf{D}-1}]$ where $\times$ is the Cartesian product. And, finally, given $\boldsymbol{n} = (n_0, \dots, n_{\mathsf{D}-1}) \in \mathbb{N}_0^{\mathsf{D}}$ and $\boldsymbol{k} = (k_0, \dots, k_{\mathsf{D}-1}) \in \mathbb{N}_0^{\mathsf{D}}$,

$$\boldsymbol{n}^{\boldsymbol{k}} \equiv n_0^{k_0} \cdots n_{\mathsf{D}-1}^{k_{\mathsf{D}-1}} \qquad \binom{\boldsymbol{n}}{\boldsymbol{k}} \equiv \binom{n_0}{k_0} \cdots \binom{n_{\mathsf{D}-1}}{k_{\mathsf{D}-1}}$$

$$\boldsymbol{k}! \equiv k_0! \cdots k_{\mathsf{D}-1}! \qquad |\boldsymbol{n}| \equiv \sum_{d=0}^{\mathsf{D}-1} |n_d|.$$

II. Channel Model

Consider N_{f} equispaced frequencies centered on f_{c} with normalized interval d_{f}, namely $f_{n_{\mathrm{f}}} = f_{\mathrm{c}}\big(1 + d_{\mathrm{f}}\big(n_{\mathrm{f}} - \frac{N_{\mathrm{f}}-1}{2}\big)\big)$ for $n_{\mathrm{f}} \in [N_{\mathrm{f}}]$. Transmitter and receiver feature uniform planar arrays (UPAs) whose dimensionalities are $N_{\mathrm{t},x} \times N_{\mathrm{t},y}$ and $N_{\mathrm{r},x} \times N_{\mathrm{r},y}$. The antenna spacings along the planar dimensions are $d_{\mathrm{t},x}$ and $d_{\mathrm{t},y}$ at the transmitter, and $d_{\mathrm{r},x}$ and $d_{\mathrm{r},y}$ at the receiver. The channel is either LOS, or subject to a specular reflection. The focus is on near-field situations, with the far field subsumed as a special case.

With the proviso that the amplitude variations across the entries are negligible, the channel connecting the $(n_{\mathrm{t},x}, n_{\mathrm{t},y})$th transmit antenna with the $(n_{\mathrm{r},x}, n_{\mathrm{r},y})$th receive antenna at frequency $f_{n_{\mathrm{f}}}$ can be normalized into [4]

$$h(\boldsymbol{n}) = \big[\boldsymbol{n} \in [\boldsymbol{N}]\big] \exp\Bigg(-\jmath \frac{2\pi}{\lambda_{\mathrm{c}}} \cdot D_{(n_{\mathrm{r},x}, n_{\mathrm{r},y}), (n_{\mathrm{t},x}, n_{\mathrm{t},y})} \left(1 + d_{\mathrm{f}} \left(n_{\mathrm{f}} - \frac{N_{\mathrm{f}} - 1}{2} \right) \right) \Bigg), \tag{2}$$

where λ_{c} is the wavelength corresponding to f_{c} while

$$\boldsymbol{n} = (n_{\mathrm{r},x}, n_{\mathrm{r},y}, n_{\mathrm{t},x}, n_{\mathrm{t},y}, n_{\mathrm{f}}) \tag{3}$$

$$\boldsymbol{N} = (N_{\mathrm{r},x}, N_{\mathrm{r},y}, N_{\mathrm{t},x}, N_{\mathrm{t},y}, N_{\mathrm{f}}), \tag{4}$$

and $D_{(n_{\mathrm{r},x}, n_{\mathrm{r},y}), (n_{\mathrm{t},x}, n_{\mathrm{t},y})}$ is the distance between the antennas. Note that the above condition on the amplitudes imposes limits on the size of the arrays relative to their separating distance, and on the bandwidth relative to f_{c}.

A. Polynomial Phase Model

As detailed in [4, Eq. 24],

$$-\frac{2\pi}{\lambda_{\mathrm{c}}} D_{(n_{\mathrm{r},x}, n_{\mathrm{r},y}), (n_{\mathrm{t},x}, n_{\mathrm{t},y})} \approx 2\pi \sum_{\boldsymbol{\ell} \in \mathcal{L}} c_{\boldsymbol{\ell}} \frac{(n_{\mathrm{r},x}, n_{\mathrm{r},y}, n_{\mathrm{t},x}, n_{\mathrm{t},y})^{\boldsymbol{\ell}}}{\boldsymbol{\ell}!} \tag{5}$$

for some coefficients $c_{\boldsymbol{\ell}}$. Here,

$$\mathcal{L} = \{\boldsymbol{\ell} \in \mathbb{N}_0^4 : |\boldsymbol{\ell}| \le L\} \tag{6}$$

is the set of degrees in the series expansion, with L regulating the modelling accuracy; $L = 1$ and $L = 2$ correspond to the common planar and parabolic wavefront models, respectively [13]. Note that $|c_{\boldsymbol{\ell}}|$ quickly decays as $|\boldsymbol{\ell}|$ grows.

From (5), the channel entries in (2) at the various frequencies can be approximated with arbitrary accuracy by

$$\big[\boldsymbol{n} \in [\boldsymbol{N}]\big] \exp\Bigg(2\pi \sum_{\boldsymbol{\ell} \in \mathcal{L}} d_{\mathrm{f}} c_{\boldsymbol{\ell}} \frac{(n_{\mathrm{r},x}, n_{\mathrm{r},y}, n_{\mathrm{t},x}, n_{\mathrm{t},y})^{\boldsymbol{\ell}}}{\boldsymbol{\ell}!} \cdot \left(\frac{1}{d_{\mathrm{f}}} + \left(n_{\mathrm{f}} - \frac{N_{\mathrm{f}} - 1}{2} \right) \right) \Bigg). \tag{7}$$

Given $a_{\boldsymbol{m}}$ and $p_{\boldsymbol{m}}(\boldsymbol{n})$ in (10), the above can be recast as

$$\big[\boldsymbol{n} \in [\boldsymbol{N}]\big] \exp\Bigg(2\pi \sum_{\boldsymbol{m}} a_{\boldsymbol{m}} p_{\boldsymbol{m}}(\boldsymbol{n}) \Bigg), \tag{11}$$

where the summation is over $\boldsymbol{m} \in \mathbb{N}_0^5$. (The definition of $p_{\boldsymbol{m}}(\boldsymbol{n})$ in the "otherwise" case in (10) is immaterial, as the corresponding coefficient is zero; it is however defined because the sequential algorithm in Sec. IV requires it.) The channel can therefore be seen as a five-dimensional polynomial phase signal: its phase is polynomial in $(n_{\mathrm{r},x}, n_{\mathrm{r},y}, n_{\mathrm{t},x}, n_{\mathrm{t},y}, n_{\mathrm{f}})$. For future use, we also define

$$\mathcal{M} = \mathcal{L} \times \{1\}, \tag{12}$$

which is the total set of polynomial degrees, i.e., the set of $\boldsymbol{m}$ associated with nonzero terms in the summation in (11).

III. Observation Model

By means of pilot transmissions, orthogonal across transmit antennas and frequencies, a noisy version of channel entries can be procured, namely

$$y(\boldsymbol{n}) = \big[\boldsymbol{n} \in [\boldsymbol{N}]\big] \big(h(\boldsymbol{n}) + w_{\mathbb{C}}(\boldsymbol{n}) \big), \tag{13}$$

where $w_{\mathbb{C}}(\boldsymbol{n}) \overset{\text{iid}}{\sim} \mathcal{N}_{\mathbb{C}}(0, \frac{1}{\mathsf{SNR}})$ is additive white Gaussian noise. Plugging (11) into (13) yields

$$y(\boldsymbol{n}) \approx \big[\boldsymbol{n} \in [\boldsymbol{N}]\big] \left(\exp\Bigg(2\pi \sum_{\boldsymbol{m}} a_{\boldsymbol{m}} p_{\boldsymbol{m}}(\boldsymbol{n}) \Bigg) + w_{\mathbb{C}}(\boldsymbol{n}) \right). \tag{14}$$

In the sequel, we explore the possibility of observing $y(\boldsymbol{n})$ only over $\{\boldsymbol{\alpha} \circ \boldsymbol{n}' + \boldsymbol{\beta} : \boldsymbol{n}' \in [\boldsymbol{N}']\} \subset [\boldsymbol{N}]$, with $\circ$ the element-wise multiplication; this amounts to uniform subsampling over antennas and frequencies (recall Fig. 1). Crucially, for every $\boldsymbol{\alpha}$ and $\boldsymbol{\beta}$ that do not collapse a dimension into a singleton, $p_{\boldsymbol{m}}(\boldsymbol{\alpha} \circ \boldsymbol{n}' + \boldsymbol{\beta})$ remains a five-dimensional polynomial.

IV. Interlude: Multidimensional Polynomial Phase Estimation

This section provides a brief summary of [14], which establishes the theoretical limits and develops a practical algorithm for multidimensional polynomial phase estimation.

Consider a D-dimensional polynomial phase signal given by $\big[\boldsymbol{n} \in [\boldsymbol{N}]\big] e^{j2\pi x(\boldsymbol{n})}$, where

$$x(\boldsymbol{n}) = \sum_{\boldsymbol{m}} a_{\boldsymbol{m}} p_{\boldsymbol{m}}(\boldsymbol{n}) \tag{15}$$

with $\boldsymbol{n} = (n_0, \dots, n_{\mathsf{D}-1})$, $\boldsymbol{m} = (m_0, \dots, m_{\mathsf{D}-1})$, and

$$p_{\boldsymbol{m}}(\boldsymbol{n}) = \frac{\boldsymbol{n}^{\boldsymbol{m}}}{\boldsymbol{m}!} + (\text{lower-degree terms}). \tag{16}$$

The coefficient $a_{\boldsymbol{m}}$ vanishes outside the set of polynomial degrees, $\mathcal{M}$. The noisy observation is

$$y(\boldsymbol{n}) = \big[\boldsymbol{n} \in [\boldsymbol{N}]\big]\big(e^{j2\pi x(\boldsymbol{n})} + w_{\mathbb{C}}(\boldsymbol{n})\big), \tag{17}$$

of which (14) is an instance for $\mathsf{D} = 5$. The goal is to estimate the polynomial coefficients $\{a_{\boldsymbol{m}}\}$ from $y(\boldsymbol{n})$.

A. Ambiguity

As the observation window is finite, to ensure that the set of polynomials $\{p_{\boldsymbol{m}}(\boldsymbol{n})\}$ is not overloaded, i.e., that the number of signals does not exceed the dimension of the space, it must hold that $\boldsymbol{m} \subset [\boldsymbol{N}]$ [14, Sec. II-B]. In addition, being devoid of injectivity, the exponential function in the observation model maps distinct polynomials onto the same signal, making the estimation fundamentally impossible. This ambiguity can be resolved by restricting the coefficients to

$$|a_{\boldsymbol{m}}| \in \big[-\tfrac{1}{2}, \tfrac{1}{2}\big) \tag{18}$$

for all $\boldsymbol{m} \in \mathcal{M}$ [14, Sec. IV-D].

B. Cramer-Rao Bound and Signal Reconstruction

The $(\boldsymbol{m}, \boldsymbol{m}')$th entry of the Fisher information matrix, $\boldsymbol{J}_{\boldsymbol{N}} \in \mathbb{R}^{|\mathcal{M}|\times|\mathcal{M}|}$, is given by

$$8\pi^2 \mathsf{SNR} \sum_{\boldsymbol{n}\in[\boldsymbol{N}]} p_{\boldsymbol{m}}(\boldsymbol{n}) p_{\boldsymbol{m}'}(\boldsymbol{n}), \tag{19}$$

as can be verified by replicating the derivation in [14, App. D]. The CRB is the inverse of $\boldsymbol{J}_{\boldsymbol{N}}$.

Once the coefficient estimates $\{\hat{a}_{\boldsymbol{m}}\}$ have been produced, the polynomial phase signal can be reconstructed as $e^{j2\pi\hat{x}(\boldsymbol{n})}$, where $\hat{x}(\boldsymbol{n}) = \sum_{\boldsymbol{m}} \hat{a}_{\boldsymbol{m}} p_{\boldsymbol{m}}(\boldsymbol{n})$. Denoting the covariance matrix of the estimator by $\boldsymbol{K}$, the reconstruction mean-square error (MSE) satisfies

$$\mathbb{E}\left[\sum_{\boldsymbol{n}\in[\boldsymbol{N}]} |e^{j2\pi\hat{x}(\boldsymbol{n})} - e^{j2\pi x(\boldsymbol{n})}|^2\right] \approx \frac{\operatorname{tr}(\boldsymbol{K}\boldsymbol{J}_{\boldsymbol{N}})}{2\,\mathsf{SNR}}, \tag{20}$$

where the approximation sharpens with the SNR. For an estimator attaining the CRB, i.e., for $\boldsymbol{K} \approx \boldsymbol{J}_{\boldsymbol{N}}^{-1}$, (20) becomes

$$\frac{|\mathcal{M}|}{2\,\mathsf{SNR}}, \tag{21}$$

which does not depend on the signal dimensionality; it depends on the cardinality of the set of polynomial degrees.

Algorithm 1 Multidimensional Polynomial Phase Estimation

procedure ESTIMATE-COEFFICIENTS($y, \mathcal{M}$)
  if $\mathcal{M} = \bigcup_{\boldsymbol{m}\in\mathcal{M}}[\boldsymbol{m}]$ **then**
    for $\boldsymbol{m} \in \mathcal{M}$ (in descending order) **do**
      $\hat{a}_{\boldsymbol{m}} \leftarrow \frac{1}{2\pi}\arg(\mu_{\boldsymbol{m}}(\mathcal{D}^{\boldsymbol{m}} y))$
      $y(\boldsymbol{n}) \leftarrow y(\boldsymbol{n}) \exp\big(-j2\pi\hat{a}_{\boldsymbol{m}} p_{\boldsymbol{m}}(\boldsymbol{n})\big)$
    end for
    return $\{\hat{a}_{\boldsymbol{m}}\}$
  else
    $\mathcal{M}' \leftarrow \bigcup_{\boldsymbol{m}\in\mathcal{M}}[\boldsymbol{m}]$
    $\hat{\boldsymbol{a}} \leftarrow$ ESTIMATE-COEFFICIENTS$(y, \mathcal{M}')$
    $\hat{\boldsymbol{a}} \leftarrow (\boldsymbol{E}\boldsymbol{J}'_{\boldsymbol{N}}\boldsymbol{E}^{\top})^{-1}\boldsymbol{E}\boldsymbol{J}'_{\boldsymbol{N}}\hat{\boldsymbol{a}}$
    return $\{\hat{a}_{\boldsymbol{m}}\}$
  end if
end procedure

C. Proposed Method

Derived in [14, Sec. IX], Algorithm 1 attains the CRB at high SNR. In it, $\mathcal{D}^{\boldsymbol{m}} \equiv \mathcal{D}_0^{m_0} \cdots \mathcal{D}_{\mathsf{D}-1}^{m_{\mathsf{D}-1}}$ where $(\mathcal{D}_d s)(\boldsymbol{n}) \equiv s(\boldsymbol{n} + \boldsymbol{e}_d)\overline{s(\boldsymbol{n})}$ with $\boldsymbol{e}_d$ the dth standard unit vector. In turn,

$$\mu_{\boldsymbol{m}}(s) = \Pi\left[\sum_{\boldsymbol{\ell}} (\Pi s)(\boldsymbol{\ell})\right] \cdot \exp\left(j \sum_{\boldsymbol{n}} u_{\boldsymbol{m}}(\boldsymbol{n}) \arg\left(s(\boldsymbol{n})\overline{\sum_{\boldsymbol{\ell}} (\Pi s)(\boldsymbol{\ell})}\right)\right), \tag{22}$$

where $(\Pi s)(\boldsymbol{n}) = e^{j\arg(s(\boldsymbol{n}))}$ for $s(\boldsymbol{n}) \neq 0$, while

$$u_{\boldsymbol{m}}(\boldsymbol{n}) = \big[\boldsymbol{n} \in [\boldsymbol{N} - \boldsymbol{m}]\big] \frac{\binom{\boldsymbol{n}+\boldsymbol{m}}{\boldsymbol{m}}\binom{\boldsymbol{N}-\boldsymbol{n}-\boldsymbol{1}}{\boldsymbol{m}}}{\binom{\boldsymbol{N}+\boldsymbol{m}}{2\boldsymbol{m}+\boldsymbol{1}}}. \tag{23}$$

Also involved in the algorithm are two additional matrices:

- Fisher information matrix for $\{a_{\boldsymbol{m}} : \boldsymbol{m} \in \mathcal{M}'\}$, where $\mathcal{M}' = \cup_{\boldsymbol{m}\in\mathcal{M}}[\boldsymbol{m}]$. Denoted by $\boldsymbol{J}'_{\boldsymbol{N}} \in \mathbb{R}^{|\mathcal{M}'|\times|\mathcal{M}'|}$, it contains $\boldsymbol{J}_{\boldsymbol{N}}$ as a submatrix; precisely, the $(\boldsymbol{m}, \boldsymbol{m}')$th entry of $\boldsymbol{J}'_{\boldsymbol{N}}$ is again given by (19), but for $\boldsymbol{m}, \boldsymbol{m}' \in \mathcal{M}'$.
- $\boldsymbol{E} \in \mathbb{R}^{|\mathcal{M}|\times|\mathcal{M}'|}$, with $(\boldsymbol{m}, \boldsymbol{m}')$th entry $[\boldsymbol{m} = \boldsymbol{m}' \in \mathcal{M}]$.

V. Extension to Partial Observation

Let us move on to the partial observation model, which generalizes the one in Sec. III. The observation through

$$\{\boldsymbol{\alpha} \circ \boldsymbol{n}' + \boldsymbol{\beta} : \boldsymbol{n}' \in [\boldsymbol{N}']\} \subset [\boldsymbol{N}], \tag{24}$$

becomes

$$y'(\boldsymbol{n}') \equiv y(\boldsymbol{\alpha} \circ \boldsymbol{n}' + \boldsymbol{\beta}) \tag{25}$$

$$= \big[\boldsymbol{n}' \in [\boldsymbol{N}']\big]\big(e^{j2\pi x'(\boldsymbol{n}')} + w'_{\mathbb{C}}(\boldsymbol{n}')\big), \tag{26}$$

where

$$x'(\boldsymbol{n}') \equiv x(\boldsymbol{\alpha} \circ \boldsymbol{n}' + \boldsymbol{\beta}) \tag{27}$$

$$= \sum_{\boldsymbol{m}} a_{\boldsymbol{m}}\, p_{\boldsymbol{m}}(\boldsymbol{\alpha} \circ \boldsymbol{n}' + \boldsymbol{\beta}) \tag{28}$$

$$= \sum_{\boldsymbol{m}} \boldsymbol{\alpha}^{\boldsymbol{m}} a_{\boldsymbol{m}}\, p'_{\boldsymbol{m}}(\boldsymbol{n}') \tag{29}$$

$$\frac{1}{2\,\mathsf{SNR}}\operatorname{tr}\Big(\boldsymbol{J}_{\boldsymbol{N}',\boldsymbol{\alpha},\boldsymbol{\beta}}^{-1}\boldsymbol{J}_{\boldsymbol{N}}\Big)=\frac{(\boldsymbol{N}')^{\mathbf{1}}}{2\,\mathsf{SNR}}\operatorname{tr}\Bigg(\Big(\tfrac{1}{(\boldsymbol{N}')^{\mathbf{1}}}\boldsymbol{D}_{\boldsymbol{\alpha}\circ\boldsymbol{N}'}\boldsymbol{J}_{\boldsymbol{N}',\boldsymbol{\alpha},\boldsymbol{\beta}}\boldsymbol{D}_{\boldsymbol{\alpha}\circ\boldsymbol{N}'}\Big)^{-1}\left(\boldsymbol{D}_{\boldsymbol{\alpha}\circ\boldsymbol{N}'}\boldsymbol{J}_{\boldsymbol{N}}\boldsymbol{D}_{\boldsymbol{\alpha}\circ\boldsymbol{N}'}\right)\Bigg) \tag{38}$$

$$=\frac{(\boldsymbol{N}')^{\mathbf{1}}}{2\,\mathsf{SNR}}\operatorname{tr}\Bigg(\Big(\tfrac{1}{(\boldsymbol{\alpha}\circ\boldsymbol{N}')^{\mathbf{1}}}\boldsymbol{D}_{\boldsymbol{\alpha}\circ\boldsymbol{N}'}\boldsymbol{J}_{\boldsymbol{\alpha}\circ\boldsymbol{N}'}\boldsymbol{D}_{\boldsymbol{\alpha}\circ\boldsymbol{N}'}\Big)^{-1}\left(\boldsymbol{D}_{\boldsymbol{\alpha}\circ\boldsymbol{N}'}\boldsymbol{J}_{\boldsymbol{N}}\boldsymbol{D}_{\boldsymbol{\alpha}\circ\boldsymbol{N}'}\right)\Bigg)+o(1)=\frac{\boldsymbol{\alpha}^{\mathbf{1}}}{2\,\mathsf{SNR}}\operatorname{tr}\big(\boldsymbol{J}_{\boldsymbol{\alpha}\circ\boldsymbol{N}'}^{-1}\boldsymbol{J}_{\boldsymbol{N}}\big)+o(1) \tag{39}$$

with

$$p'_{\boldsymbol{m}}(\boldsymbol{n}')\equiv\frac{1}{\boldsymbol{\alpha}^{\boldsymbol{m}}}\,p_{\boldsymbol{m}}(\boldsymbol{\alpha}\circ\boldsymbol{n}'+\boldsymbol{\beta}) \tag{30}$$

$$=\frac{(\boldsymbol{n}')^{\boldsymbol{m}}}{\boldsymbol{m}!}+(\text{terms with lower degree}) \tag{31}$$

while $w'_{\mathbb{C}}(\boldsymbol{n}')\equiv w_{\mathbb{C}}(\boldsymbol{\alpha}\circ\boldsymbol{n}'+\boldsymbol{\beta})$.

A. Ambiguity

Applying the result in Sec. IV-A, the ambiguity can be eliminated provided that $\mathcal{M}\subset[\boldsymbol{N}']$ and

$$|a_{\boldsymbol{m}}|\in\tfrac{1}{\boldsymbol{\alpha}^{\boldsymbol{m}}}\big[-\tfrac{1}{2},\tfrac{1}{2}\big) \tag{32}$$

for all $\boldsymbol{m}\in\mathcal{M}$. These ambiguity-free conditions are more exacting than (18).

B. Cramer-Rao Bound and Its Asymptotic Expansion

Consider $\boldsymbol{J}_{\boldsymbol{N}',\boldsymbol{\alpha},\boldsymbol{\beta}}\in\mathbb{R}^{|\mathcal{M}|\times|\mathcal{M}|}$ for the partial observation model. As $\boldsymbol{N}'$ and $\boldsymbol{N}$ grow with a fixed ratio, the $(\boldsymbol{m},\boldsymbol{m}')$th entry of $\boldsymbol{J}_{\boldsymbol{N}',\boldsymbol{\alpha},\boldsymbol{\beta}}$ expands as

$$8\pi^2\mathsf{SNR}\,\boldsymbol{\alpha}^{\boldsymbol{m}+\boldsymbol{m}'}\sum_{\boldsymbol{n}\in[\boldsymbol{N}']}p'_{\boldsymbol{m}}(\boldsymbol{n})p'_{\boldsymbol{m}'}(\boldsymbol{n}) \tag{33}$$

$$=8\pi^2\mathsf{SNR}\,\boldsymbol{\alpha}^{\boldsymbol{m}+\boldsymbol{m}'} \tag{34}$$

$$\cdot\sum_{\boldsymbol{n}'\in[\boldsymbol{N}']}\left(\frac{(\boldsymbol{n}')^{\boldsymbol{m}+\boldsymbol{m}'}}{\boldsymbol{m}!\boldsymbol{m}'!}+(\text{terms with lower degree})\right)$$

$$=8\pi^2\mathsf{SNR}\,\boldsymbol{\alpha}^{\boldsymbol{m}+\boldsymbol{m}'}\frac{(\boldsymbol{N}')^{\boldsymbol{m}+\boldsymbol{m}'+\mathbf{1}}}{\boldsymbol{m}!\boldsymbol{m}'!(\boldsymbol{m}+\boldsymbol{m}'+\mathbf{1})^{\mathbf{1}}}\big(1+o(1)\big) \tag{35}$$

$$=\frac{1+o(1)}{\boldsymbol{\alpha}^{\mathbf{1}}}\cdot 8\pi^2\mathsf{SNR}\,\frac{(\boldsymbol{\alpha}\circ\boldsymbol{N}')^{\boldsymbol{m}+\boldsymbol{m}'+\mathbf{1}}}{\boldsymbol{m}!\boldsymbol{m}'!(\boldsymbol{m}+\boldsymbol{m}'+\mathbf{1})^{\mathbf{1}}}. \tag{36}$$

Introducing a diagonal matrix $\boldsymbol{D}_{\boldsymbol{N}}\in\mathbb{R}^{|\mathcal{M}|\times|\mathcal{M}|}$ whose $\boldsymbol{m}$th diagonal entry is $\boldsymbol{N}^{-\boldsymbol{m}}$, it can be verified that the $(\boldsymbol{m},\boldsymbol{m}')$th entries of both $\frac{1}{(\boldsymbol{N}')^{\mathbf{1}}}\boldsymbol{D}_{\boldsymbol{\alpha}\circ\boldsymbol{N}'}\boldsymbol{J}_{\boldsymbol{N}',\boldsymbol{\alpha},\boldsymbol{\beta}}\boldsymbol{D}_{\boldsymbol{\alpha}\circ\boldsymbol{N}'}$ and $\frac{1}{(\boldsymbol{\alpha}\circ\boldsymbol{N}')^{\mathbf{1}}}\boldsymbol{D}_{\boldsymbol{\alpha}\circ\boldsymbol{N}'}\boldsymbol{J}_{\boldsymbol{\alpha}\circ\boldsymbol{N}'}\boldsymbol{D}_{\boldsymbol{\alpha}\circ\boldsymbol{N}'}$ equal

$$8\pi^2\mathsf{SNR}\frac{1}{\boldsymbol{m}!\boldsymbol{m}'!(\boldsymbol{m}+\boldsymbol{m}'+\mathbf{1})^{\mathbf{1}}}+o(1). \tag{37}$$

It follows, via perturbation theory [15, Thm. 2.3.4], that the $(\boldsymbol{m},\boldsymbol{m}')$th entries of $(\frac{1}{(\boldsymbol{N}')^{\mathbf{1}}}\boldsymbol{D}_{\boldsymbol{\alpha}\circ\boldsymbol{N}'}\boldsymbol{J}_{\boldsymbol{N}',\boldsymbol{\alpha},\boldsymbol{\beta}}\boldsymbol{D}_{\boldsymbol{\alpha}\circ\boldsymbol{N}'})^{-1}$ and $(\frac{1}{(\boldsymbol{\alpha}\circ\boldsymbol{N}')^{\mathbf{1}}}\boldsymbol{D}_{\boldsymbol{\alpha}\circ\boldsymbol{N}'}\boldsymbol{J}_{\boldsymbol{\alpha}\circ\boldsymbol{N}'}\boldsymbol{D}_{\boldsymbol{\alpha}\circ\boldsymbol{N}'})^{-1}$ differ by $o(1)$.

C. Reconstruction MSE and Its Asymptotic Expansion

From the property of the trace operator, we have (38)–(39) where the dependence on $\boldsymbol{\beta}$ has been relegated to the nuisance term. The leading term above, in turn, can be factored as

$$\underbrace{\frac{|[\boldsymbol{N}]|}{|[\boldsymbol{N}']|}}_{\text{first}}\cdot\underbrace{\frac{1}{|\mathcal{M}|}\operatorname{tr}\left(\left(\frac{\boldsymbol{J}_{\boldsymbol{\alpha}\circ\boldsymbol{N}'}}{(\boldsymbol{\alpha}\circ\boldsymbol{N}')^{\mathbf{1}}}\right)^{-1}\left(\frac{\boldsymbol{J}_{\boldsymbol{N}}}{\boldsymbol{N}^{\mathbf{1}}}\right)\right)}_{\text{second}}\cdot\underbrace{\frac{|\mathcal{M}|}{2\,\mathsf{SNR}}}_{\text{third}}, \tag{40}$$

with the following interpretation:

- The first factor represents the rise in MSE due to the reduction in the number of observations. This term is equal to or larger than 1, but it can be counterbalanced by increasing the power of the $|[\boldsymbol{N}']|$ observations, i.e., through pilot power boosting.
- The second factor represents the rise in MSE due to the reduction in window size. As shown in App. A, this term is equal to or greater than $1+o(1)$. For interpolation specifically, i.e., for $\boldsymbol{\alpha}\circ\boldsymbol{N}'=\boldsymbol{N}$, this term equals 1.
- The third factor is the full-observation MSE, as per (21).

The first factor therefore magnifies the full-observation MSE in both interpolation and extrapolation. The second factor further magnifies it in the case of extrapolation.

TABLE I
PARAMETERS FOR NUMERICAL EVALUATION.

Parameters	Value
Wavelength	1 cm
Frequency spacing	6 MHz
Number of frequency grids	64
Distance between array centers	10 m
Array dimensionalities	16×16 UPA
Array spacings	Half-wavelength
Array orientations	Uniformly random
L controlling modelling accuracy	2

VI. PERFORMANCE EVALUATION

Let us consider the settings in Table I, whereby the channel has a dimensionality of $16\times16\times16\times16\times64=4$ million entries. The evaluated cases are:

- Full observation over $[\boldsymbol{N}]$.
- Interpolation from observation over $\{\boldsymbol{\alpha}\circ\boldsymbol{n}'+\boldsymbol{\beta}:\boldsymbol{n}'\in[\boldsymbol{N}']\}$ with $\boldsymbol{\alpha}=(1,1,2,2,2)$, $\boldsymbol{\beta}=\mathbf{0}$, and $\boldsymbol{N}'=\big(N_{\mathrm{r},x},N_{\mathrm{r},y},\frac{N_{\mathrm{t},x}}{2},\frac{N_{\mathrm{t},y}}{2},\frac{N_{\mathrm{f}}}{2}\big)$. This corresponds to emitting pilots from every other antenna on each planar dimension at the transmit array, and on every other frequency band.
- Extrapolation from observation over $\{\boldsymbol{\alpha}\circ\boldsymbol{n}'+\boldsymbol{\beta}:\boldsymbol{n}'\in[\boldsymbol{N}']\}$ with $\boldsymbol{\alpha}=\mathbf{1}$, $\boldsymbol{\beta}=\mathbf{0}$, and $\boldsymbol{N}'=\big(N_{\mathrm{r},x},N_{\mathrm{r},y},\frac{N_{\mathrm{t},x}}{2},\frac{N_{\mathrm{t},y}}{2},\frac{N_{\mathrm{f}}}{2}\big)$. The number of observations is identical to that of the interpolation.

The channels are generated via (2), with the exact spherical shape. The per-entry MSEs, obtained numerically, are presented in Fig. 2. The least-squares estimator under a full observation serves as benchmark (under partial observation, it is infeasible as the model is underdetermined); it corresponds to the noisy observation itself, with an MSE of $\frac{1}{\mathsf{SNR}}$.

Turning to the wavefront estimator, the full-observation MSE exhibits a threshold behavior, approaching (21) beyond it. For growing SNR, the MSE eventually saturates owing

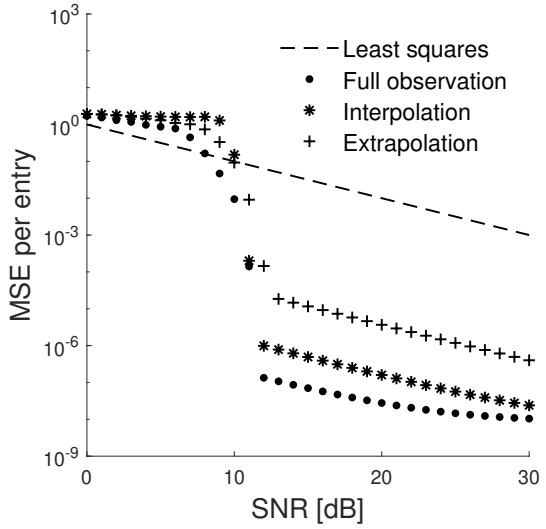

Fig. 2. Reconstruction MSE (averaged over 100 realizations of the geometric parameters and the noise) as a function of SNR.

to the mismatch between the actual spherical shape of the wavefronts and the polynominal expansion of that shape assumed by the estimator. With interpolation, the pilot overhead is reduced by a factor of 8, at the expense—from the first factor in (40)—of a 9-dB penalty relative to a full observation. To the extent that the pilot power can be magnified, this loss would be recovered; if the pilot power is boosted by 9 dB, the loss is fully erased. Put differently, by concentrating the same pilot energy of the full observation case onto a subset of pilots, the same channel estimation accuracy can be attained with a reduced overhead. This directly translates to a higher spectral efficiency.

In the extrapolation case, the second factor in (40) further penalizes the MSE. A uniform pilot disposition across antennas and frequencies is thus desirable to prevent this penalty.

VII. Acknowledgment

Heedong Do and Namyoon Lee are supported by the National Research Foundation of Korea (NRF) funded by the Korea government through Ministry of Science and ICT (MSIT) under Grant RS-2023-00208552. A. Lozano is supported by ICREA and by the Maria de Maeztu Units of Excellence Programme CEX2021-001195-M funded by MICIU/AEI/10.13039/501100011033.

Appendix A

From $\boldsymbol{D}_{\boldsymbol{\alpha}\circ\boldsymbol{N}'}\boldsymbol{D}_{\boldsymbol{N}^{\boldsymbol{m}}}^{-1}$ being a diagonal matrix whose $\boldsymbol{m}$th diagonal entry is $\frac{\boldsymbol{N}^{\boldsymbol{m}}}{(\boldsymbol{\alpha}\circ\boldsymbol{N}')^{\boldsymbol{m}}} \geq 1$, and from App. B,

$$\boldsymbol{D}_{\boldsymbol{\alpha}\circ\boldsymbol{N}'}\boldsymbol{J}_{\boldsymbol{N}}\boldsymbol{D}_{\boldsymbol{\alpha}\circ\boldsymbol{N}'} \tag{41}$$

$$= \boldsymbol{D}_{\boldsymbol{\alpha}\circ\boldsymbol{N}'}\boldsymbol{D}_{\boldsymbol{N}}^{-1}(\boldsymbol{D}_{\boldsymbol{N}}\boldsymbol{J}_{\boldsymbol{N}}\boldsymbol{D}_{\boldsymbol{N}})\boldsymbol{D}_{\boldsymbol{N}}^{-1}\boldsymbol{D}_{\boldsymbol{\alpha}\circ\boldsymbol{N}'} \tag{42}$$

$$\geq \boldsymbol{D}_{\boldsymbol{N}}\boldsymbol{J}_{\boldsymbol{N}}\boldsymbol{D}_{\boldsymbol{N}}. \tag{43}$$

Hence,

$$\frac{1}{|\mathcal{M}|}\operatorname{tr}\left(\left(\frac{\boldsymbol{J}_{\boldsymbol{\alpha}\circ\boldsymbol{N}'}}{(\boldsymbol{\alpha}\circ\boldsymbol{N}')^{\mathbf{1}}}\right)^{-1}\left(\frac{\boldsymbol{J}_{\boldsymbol{N}}}{\boldsymbol{N}^{\mathbf{1}}}\right)\right) \tag{44}$$

$$= \frac{1}{|\mathcal{M}|}\operatorname{tr}\Big(\big(\tfrac{1}{(\boldsymbol{\alpha}\circ\boldsymbol{N}')^{\mathbf{1}}}\boldsymbol{D}_{\boldsymbol{\alpha}\circ\boldsymbol{N}'}\boldsymbol{J}_{\boldsymbol{\alpha}\circ\boldsymbol{N}'}\boldsymbol{D}_{\boldsymbol{\alpha}\circ\boldsymbol{N}'}\big)^{-1} \cdot \big(\tfrac{1}{\boldsymbol{N}^{\mathbf{1}}}\boldsymbol{D}_{\boldsymbol{\alpha}\circ\boldsymbol{N}'}\boldsymbol{J}_{\boldsymbol{N}}\boldsymbol{D}_{\boldsymbol{\alpha}\circ\boldsymbol{N}'}\big)\Big) \tag{45}$$

$$\geq \frac{1}{|\mathcal{M}|}\operatorname{tr}\Big(\big(\tfrac{1}{(\boldsymbol{\alpha}\circ\boldsymbol{N}')^{\mathbf{1}}}\boldsymbol{D}_{\boldsymbol{\alpha}\circ\boldsymbol{N}'}\boldsymbol{J}_{\boldsymbol{\alpha}\circ\boldsymbol{N}'}\boldsymbol{D}_{\boldsymbol{\alpha}\circ\boldsymbol{N}'}\big)^{-1} \cdot \big(\tfrac{1}{\boldsymbol{N}^{\mathbf{1}}}\boldsymbol{D}_{\boldsymbol{N}}\boldsymbol{J}_{\boldsymbol{N}}\boldsymbol{D}_{\boldsymbol{N}}\big)\Big) \tag{46}$$

$$= 1 + o(1), \tag{47}$$

where the last step follows from the $(\boldsymbol{m},\boldsymbol{m}')$th entries of both $\frac{1}{(\boldsymbol{\alpha}\circ\boldsymbol{N}')^{\mathbf{1}}}\boldsymbol{D}_{\boldsymbol{\alpha}\circ\boldsymbol{N}'}\boldsymbol{J}_{\boldsymbol{\alpha}\circ\boldsymbol{N}'}\boldsymbol{D}_{\boldsymbol{\alpha}\circ\boldsymbol{N}'}$ and $\frac{1}{\boldsymbol{N}^{\mathbf{1}}}\boldsymbol{D}_{\boldsymbol{N}}\boldsymbol{J}_{\boldsymbol{N}}\boldsymbol{D}_{\boldsymbol{N}}$ equaling (37).

Appendix B

Consider a positive definite matrix $\boldsymbol{A}$ and a diagonal matrix $\boldsymbol{D}$ whose diagonal entries are equal to or larger than 1. Then,

$$\{\boldsymbol{x} : \boldsymbol{x}^\top\boldsymbol{A}^{-1}\boldsymbol{x} \leq 1\} \subset \{\boldsymbol{D}\boldsymbol{x} : \boldsymbol{x}^\top\boldsymbol{A}^{-1}\boldsymbol{x} \leq 1\} \tag{48}$$

$$\Leftrightarrow \{\boldsymbol{x} : \boldsymbol{x}^\top\boldsymbol{A}^{-1}\boldsymbol{x} \leq 1\} \subset \{\boldsymbol{x} : \boldsymbol{x}^\top(\boldsymbol{D}\boldsymbol{A}\boldsymbol{D})^{-1}\boldsymbol{x} \leq 1\} \tag{49}$$

$$\Leftrightarrow \boldsymbol{A} \leq \boldsymbol{D}\boldsymbol{A}\boldsymbol{D}, \tag{50}$$

where the last step follows from [16, Example 2.18].

References

[1] Q. Sun, D. Cox, A. Lozano, and H. C. Huang, "Training-based channel estimation for continuous flat fading BLAST," in *IEEE Int'l Conf. Commun.*, 2002, pp. 325–329.

[2] R. W. Heath, Jr. and A. Lozano, *Foundations of MIMO Communication*. Cambridge University Press, 2018.

[3] W. U. Bajwa, J. Haupt, A. M. Sayeed, and R. Nowak, "Compressed channel sensing: A new approach to estimating sparse multipath channels," *Proc. IEEE*, vol. 98, no. 6, pp. 1058–1076, 2010.

[4] H. Do, N. Lee, and A. Lozano, "Estimation of near-field line-of-sight channels: a multidimensional polynomial phase approach," in *Proc. Asilomar Conf. Signals Syst. Comput.*, 2024.

[5] M. D. Larsen, A. L. Swindlehurst, and T. Svantesson, "Performance bounds for MIMO-OFDM channel estimation," *IEEE Trans. Signal Process.*, vol. 57, no. 5, pp. 1901–1916, 2009.

[6] F. Rottenberg, T. Choi, P. Luo, C. J. Zhang, and A. F. Molisch, "Performance analysis of channel extrapolation in FDD massive MIMO systems," *IEEE Trans. Wireless Commun.*, vol. 19, no. 4, pp. 2728–2741, 2020.

[7] Z. Zhang, J. Zhang, Y. Zhang, L. Yu, and G. Liu, "AI-based time-, frequency-, and space-domain channel extrapolation for 6G: Opportunities and challenges," *IEEE Veh. Technol. Mag.*, vol. 18, no. 1, pp. 29–39, 2023.

[8] H. Do, N. Lee, and A. Lozano, "Reconfigurable ULAs for line-of-sight MIMO transmission," *IEEE Trans. Wireless Commun.*, vol. 20, no. 5, pp. 2933–2947, 2021.

[9] ——, "Line-of-sight MIMO via intelligent reflecting surface," *IEEE Trans. Wireless Commun.*, vol. 22, no. 6, pp. 4215–4231, 2023.

[10] A. Guerra, F. Guidi, D. Dardari, and P. M. Djurić, "Near-field tracking with large antenna arrays: Fundamental limits and practical algorithms," *IEEE Trans. Signal Process.*, vol. 69, pp. 5723–5738, 2021.

[11] P. Ramezani, A. Kosasih, A. Irshad, and E. Björnson, "Exploiting the depth and angular domains for massive near-field spatial multiplexing," *IEEE BITS Inform. Theory Mag.*, vol. 3, no. 1, pp. 14–26, 2023.

[12] A. Pizzo, A. Lozano, S. Rangan, and T. L. Marzetta, "Wide-aperture MIMO via reflection off a smooth surface," *IEEE Trans. Wireless Commun.*, vol. 22, no. 8, pp. 5229–5239, 2023.

[13] H. Do, N. Lee, and A. Lozano, "Parabolic wavefront model for line-of-sight MIMO channels," *IEEE Trans. Wireless Commun.*, vol. 22, no. 11, pp. 7620–7634, 2023.

[14] ——, "Multidimensional polynomial phase estimation," *arXiv preprint arXiv:2411.06885*, 2024.

[15] G. H. Golub and C. F. Van Loan, *Matrix computations*. JHU press, 2013.

[16] S. P. Boyd and L. Vandenberghe, *Convex optimization*. Cambridge university press, 2004.